ACS OMEGA

http://pubs.acs.org/journal/acsodf

Article

Impact of Low Temperatures on the Lithiation and Delithiation Properties of Si-Based Electrodes in Ionic Liquid Electrolytes

Yasuhiro Domi, Hiroyuki Usui, Tasuku Hirosawa, Kai Sugimoto, Takuma Nakano, Akihiro Ando, and Hiroki Sakaguchi*

Cite This: *ACS Omega* 2022, 7, 15846−15853

Read Online

ACCESS | Metrics & More | Article Recommendations | Supporting Information

ABSTRACT: Lithium-ion batteries are used in various extreme environments, such as cold regions and outer space; thus, improvements in energy density, safety, and cycle life in these environments are urgently required. We investigated changes in the charge and discharge properties of Si-based electrodes in ionic liquid electrolytes with decreasing temperature and the cycle life at low temperature. The reversible capacity at low temperature was determined by the properties of the surface film on the electrodes and/or the ionic conductivity of the electrolytes. The electrode coated with a surface film formed at a low temperature exhibited insufficient capacity. In contrast, a Si-only electrode precoated with the surface film at room temperature exhibited a cycle life at low temperatures in ionic liquid electrolytes longer than that in conventional organic liquid electrolytes. Doping phosphorus into Si led to improved cycling performance, and its impact was more noticeable at lower temperatures.

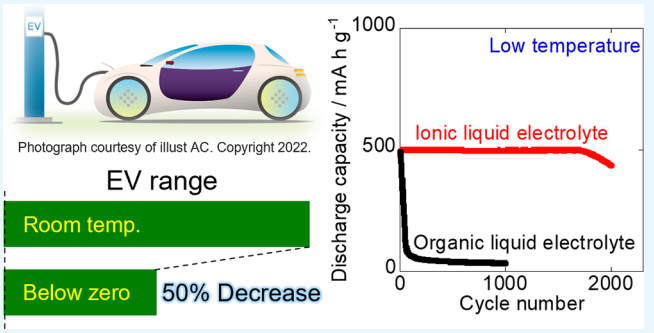

1. INTRODUCTION

Since the commercialization of lithium-ion batteries (LIBs), the importance of rechargeable batteries continues to increase; for example, LIBs are widely used as power sources in devices ranging from portable electronics to electric vehicles (EVs), mounted on microsatellites, and used as a power source for space applications.[1] The EV range in cold regions drops by half compared to their range at normal temperatures. Additionally, LIBs will contribute to the electrification of aircraft in the future.[2] Thus, LIBs will be used in extreme environments, including those that have low and high temperatures, are under vacuum, and experience radiation exposure; therefore, it is essential to investigate the electrochemical performances of LIBs in various environments and improve their energy density, safety, and cycle life.

Silicon (Si) is an up-and-coming material for negative electrodes in next-generation LIBs because its theoretical capacity (3580 mA h g^{-1} for $Li_{3.75}Si$) is higher than that of currently used graphite (372 mA h g^{-1} for $Li_{0.17}C$).[3−5] Nevertheless, the poor cycling performance of Si-based electrodes is an obstacle to their practical use, which can be attributed to following: the significant volume change during lithiation and delithiation which generates considerable stress and high strain in active materials; high electrical resistivity; and a low Li^+ diffusion coefficient.[5−9] Various attempts have been made to address such issues, for example, synthesizing nanosized Si materials to prevent the occurrence of surface cracking and fracture;[7,10,11] reducing the electrical resistivity of Si by coating it with carbon materials;[12,13] fabricating composite electrodes to cover the shortcomings of Si;[14−17] doping Si with impurities, such as phosphorus (P), boron, antimony, or arsenic, to adjust its properties, including its electrical resistivity, Li distribution, crystallinity, and morphology;[18−24] preparing silicides to give ductility and electronic conductivity specific to metals;[25−27] and the prelithiation of Si to increase the initial Coulombic efficiency.[28−31]

Electrolytes dominate the charge and discharge properties and safety of rechargeable batteries.[31−36] A battery with an enhanced energy density increases the risk of ignition and explosion, and therefore, nonflammable electrolytes are required. In particular, the electrolyte viscosity increases with decreasing temperature, leading to an increase in internal resistance. Additionally, low temperatures result in higher rates of Li dendrite formation, decreasing the safety of a battery.[37,38] To improve battery safety, fluorine-containing organic liquid electrolytes have been applied to graphite negative electrodes.[39,40] In contrast, ionic liquid electrolytes that have superior physicochemical properties have been studied for Si-based electrodes.[41−44] A certain ionic liquid electrolyte contributes to

Received: February 16, 2022
Accepted: April 13, 2022
Published: April 26, 2022

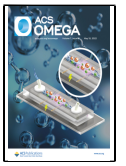

an improvement in not only the safety but also the lithiation−delithiation properties of a battery.[20,21,45,46] Consequently, LIBs using ionic liquid electrolytes have been increasingly studied as next-generation rechargeable batteries.

While the electrochemical performances of Si-based electrodes at room temperature in various ionic liquid electrolytes and at low temperature in conventional organic liquid electrolytes have been investigated,[21,22,47−50] there are few reports on their performances at low temperatures in the ionic liquid electrolytes. Considering the use of LIBs in cold regions and outer space, it is important to understand and improve their low-temperature characteristics. In the present study, we investigated changes in the lithiation and delithiation properties of a Si electrode with decreasing temperature in ionic liquid electrolytes and in the cycle life at low temperatures. We also demonstrated that a P-doped Si electrode that exhibited superior electrochemical performance at room temperature showed superior low-temperature characteristics.[19,21,23] Herein, we used lithium bis(fluorosulfonyl)amide (LiFSA) dissolved in *N*-methyl-*N*-propylpyrrolidinium bis(fluorosulfonyl)amide (Py13-FSA) and LiFSA dissolved in 1-ethyl-3-methylimidazolium bis(fluorosulfonyl)amide (EMI-FSA) as ionic liquid electrolyte. The Si electrodes exhibited superior cycle life and better rate performance in the former and latter electrolytes, respectively.

2. EXPERIMENTAL SECTION

2.1. Materials. Elemental Si (99.9%) was obtained from FUJIFILM Wako Pure Chemical Corporation, Ltd. and was mechanically milled by a planetary high-energy ball mill (P-6, Fritsch). The active material of 100 ppm P-doped Si powder (Silgrain e-Si, Elkem ASA) was used as received. LiFSA (99%), 1 mol dm^{-3} (M) lithium hexafluorophosphate ($LiPF_6$) dissolved in a 1:1 (by volume) mixture of ethylene carbonate (EC) and diethyl carbonate (DEC) and 1 M lithium bis(trifluoromethanesulfonyl)amide (LiTFSA) dissolved in propylene carbonate (PC) were purchased from Kishida Chemical Co., Ltd. Ionic liquids of Py13-FSA (97%) and EMI-FSA (97%) were supplied by Kanto Chemical Co., Inc. The chemical structures of the above Li salts, ionic liquids, and organic liquids are displayed in Figure S1 (Supporting Information).

2.2. Electrode Fabrication and Cell Assembly. Si- and P-doped Si electrodes were fabricated by the gas-deposition (GD) method without any binder and/or conductive assistance. We used copper foil as the current collector. The loading amount of active material on the Cu substrate was 30 ± 3 μg. Other detailed GD conditions are described in our previous papers.[19,21]

We assembled coin cells (2032-type) using the Si- or P-doped Si electrode as the working electrode. Details of the counter electrode and separator are reported in our previous papers.[20,21,51] We used 1 M LiFSA/Py13-FSA and 1 M LiFSA/EMI-FSA as the ionic liquid electrolyte and 1 M $LiPF_6$/EC +DEC (1:1, vol %) and 1 M LiTFSA/PC as the organic liquid electrolyte. We assembled the cell and prepared the electrolyte in an Ar-filled glovebox (Miwa MFG, DBO-2.5LNKP-TS) with an oxygen content less than 1 ppm and a dew point below −90 °C.

2.3. Charge−Discharge Testing. Charge−discharge testing was galvanostatically performed using an electrochemical measurement system (HJ-1001SD8, Hokuto Denko Co., Ltd.) and a thermostatic chamber (SH-242, ESPEC Corp.). Precycling was conducted as follows to form a good surface film on the electrode; the Si- or P-doped Si electrode was charged from open circuit voltage (OCV) to 0.500 V vs Li^+/Li at 0.1*C*, maintained at 0.500 V vs Li^+/Li for 12 h, and then discharged to 2.000 V vs Li^+/Li at 0.1*C* (1*C*: 3600 mA g^{-1}).[15] That is, the charge and discharge procedures of the precycling were conducted by the constant current (CC) and constant voltage (CV) mode and CC mode, respectively. Charge−discharge testing was performed at various temperatures between 303 and 233 K, whereas low-temperature testing was conducted at 263 K. The charge capacity limit was determined by controlling the limitation time to approximately 17 and 8 min for the 1000 and 500 mA h g^{-1} capacity limitation, respectively. The *C* rate was set at 1*C* and the current density per area of 1*C* was 108 μA cm^{-2}. Other detailed conditions are described in our previous paper.[21]

2.4. Ionic Conductivity Measurement. The ionic conductivity (σ) of the various electrolytes was investigated by electrochemical impedance spectroscopy (EIS, Compact-Stat, Ivium Technologies B.V.) in the temperature range of 303 to 233 K. A cell equipped with two Pt electrodes was used in an Ar atmosphere. The cell constant was calibrated using a KCl standard solution. The cell was placed in the thermostatic chamber at each temperature for at least 1 h. EIS measurements were then performed by applying a sine wave with an amplitude of 10 mV over a frequency range of 10 kHz to 50 Hz.

3. RESULTS AND DISCUSSION

3.1. Lithiation−Delithiation Properties of a Si Electrode at Various Temperatures. Figure 1a shows the schematic control flow for charge−discharge testing with decreasing temperature. We performed testing for five cycles

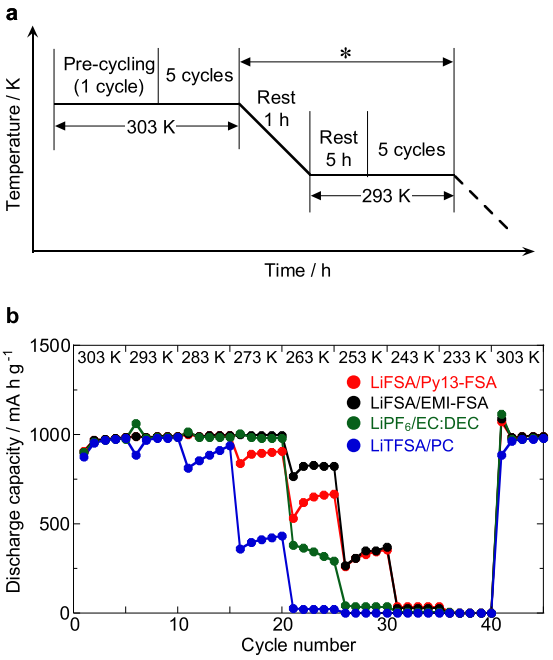

Figure 1. (a) Schematic procedure of the charge−discharge test with decreasing temperature. The process indicated by asterisks was performed repeatedly. (b) Dependence of the discharge capacity of Si electrodes on the temperature at 1*C* in various electrolytes with a charge capacity limitation of 1000 mA h g^{-1}.

https://doi.org/10.1021/acsomega.2c00947
ACS Omega 2022, 7, 15846−15853

after precycling at room temperature (303 K). Then the temperature was decreased by 10 K in 1 h and held for 5 h at 293 K to bring the temperature of the whole cell to 293 K. After that, we conducted charge−discharge testing for five cycles at 293 K. The set of the processes indicated by the asterisk in Figure 1a was repeated until reaching 233 K. Finally, the testing was again carried out at 303 K. Figure 1b shows changes in the discharge capacity of a Si electrode with a decrease in temperature in various electrolytes. The electrode could maintain a reversible capacity of 1000 mA h g^{-1} in all electrolytes until reaching 293 K. It was expected that the Si electrode at low temperatures in PC-based electrolytes would show superior charge and discharge properties because PC remains in a liquid state between 224 and 515 K.[52−54] However, contrary to our expectations, the capacity in LiTFSA/PC was the lowest at a relatively high temperature of 283 K. The discharge capacity of 1000 mA h g^{-1} in LiFSA/Py13-FSA and LiFSA/EMI-FSA or $LiPF_6$/EC+DEC began to decrease at 273 and 263 K, respectively. The Si electrode exhibited almost no reversible capacity at 243 and 233 K regardless of the electrolyte, whereas the capacity recovered to 1000 mA h g^{-1} when retuned to 303 K, implying no electrode degradation.

Figure 2 provides each fifth differential capacity (dQ/dV) plot at various temperatures in the ionic liquid electrolyte (1 M LiFSA/Py13-FSA) and organic liquid electrolyte (1 M LiTFSA/PC). The corresponding charge/discharge curve is shown in Figure S2. Whereas the degree of polarization increased as the temperature decreased in the organic liquid electrolyte, it was suppressed in the ionic liquid electrolyte. That is, the internal resistance hardly increased in the ionic liquid electrolyte even at low temperature. The internal resistance includes the solution resistance and interfacial resistance, which consists of the surface film resistance and charge transfer resistance between the Si electrode and electrolyte solution. An increase in the internal resistance causes a decrease in battery voltage. To clarify the solution resistance, we investigated σ with EIS.

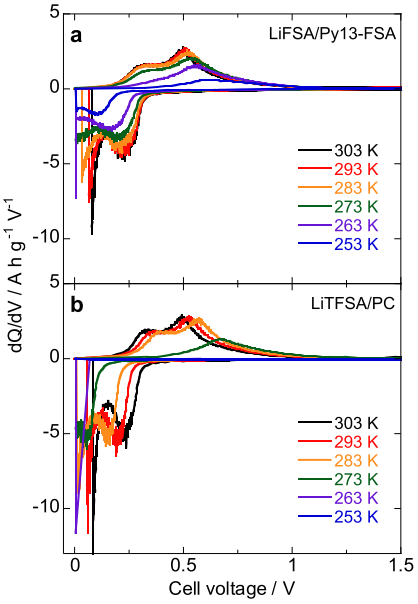

Figure 2. Each fifth dQ/dV plot of the Si electrodes at various temperatures in (a) 1 M LiFSA/Py13-FSA and (b) 1 M LiTFSA/PC. The corresponding charge/discharge curve is shown in Figure S2.

Figure 3 and Table 1 display the σ and activation energy (E_a) values of various electrolytes. Because the ionic liquid is not in the liquid state but is in a gel-like state when evaluated at the lowest temperature (233 K), the σ at 233 K is not shown in Figure 3a. Additionally, the ln σ at 243 K was out of correlation of Figure 3b; thus, we show the Arrhenius plot between 303 and 253 K. E_a was calculated from the equation $\ln \sigma = -E_a/RT + C$, where R is the gas constant and C is a constant. Although the obtained σ at room temperature was in close agreement with the reported values,[55−59] the E_a estimated from room temperature to low temperatures was several kJ mol^{-1} higher than the value evaluated from room temperature to high temperatures, implying slower ion conduction at low temperatures.[33,56] Additionally, the E_a for the ionic liquid electrolytes was higher than that for the organic liquid electrolytes. This result indicated the faster ion conductive behavior of the organic liquid electrolytes over the temperature range due to their lower viscosities.[60] The σ of LiTFSA/PC was almost the same as that of LiFSA/Py13-FSA at 283 K. Thus, the capacity decay in LiTFSA/PC at 283 K (Figure 1b) did not result from σ but should be attributed to the difference in properties of the surface film formed on the electrode, that is, the higher interfacial resistance in LiTFSA/PC.

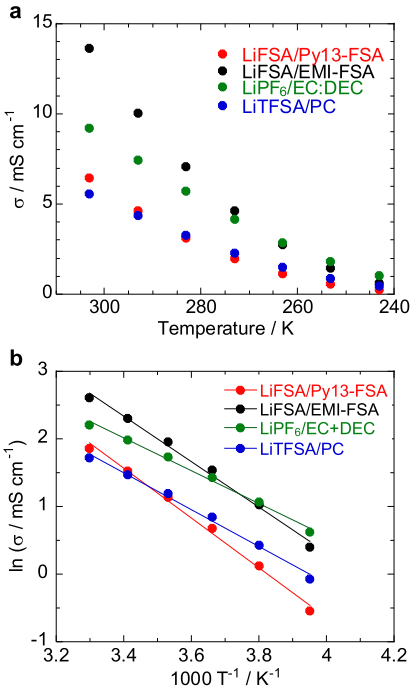

Figure 3. (a) Temperature dependence of the ionic conductivity (σ) between 303 and 243 K and (b) its Arrhenius plot.

Table 1. Activation Energy of Various Electrolytes Estimated by Figure 3b

electrolyte	E_a (kJ mol^{-1})
LiFSA/Py13-FSA	30.6
LiFSA/EMI-FSA	28.0
$LiPF_6$/EC+DEC	20.1
LiTFSA/PC	22.8

https://doi.org/10.1021/acsomega.2c00947
ACS Omega 2022, 7, 15846−15853

3.2. Cycle Life of the Si Electrode at Low Temperature.

Figure 4a,b shows the schematic procedure for the cycle life test of the Si electrode and the obtained cycle life, respectively. Precycling was performed at (i) 303 and (ii) 263 K. Figure S3 displays the relationship between the potential and capacity when precycling at each temperature. While the charge capacity was approximately 870 and 570 mA h g^{-1} in the CC and CV modes at 303 K, respectively, it was 350 and 440 mA h g^{-1} in the CC and CV modes at 263 K, respectively. Precycling at 303 K enabled a discharge capacity of 500 mA h g^{-1} to be maintained over 500 cycles. In contrast, the capacity did not reach 500 mA h g^{-1} and faded with precycling at 263 K. These results revealed that the surface film formed at room temperature gave the Si electrode superior lithiation and delithiation properties, whereas the surface film formed at the low temperature had a low σ and an inhomogeneous thickness and/or components. The same should apply to the Li metal as the counter electrode. When the cycle test at the low temperature was performed with five cycles at 263 K after precycling at 303 K, the cycling performance was poor (data not shown). This result indicates that the five cycles at 303 K after precycling contribute to stabilizing the surface film; in other words, the slight formation of a surface film should occur during those five cycles.[50] Hence, we investigated the cycle life of Si-based electrodes at the low temperature after precycling and five cycles at 303 K.

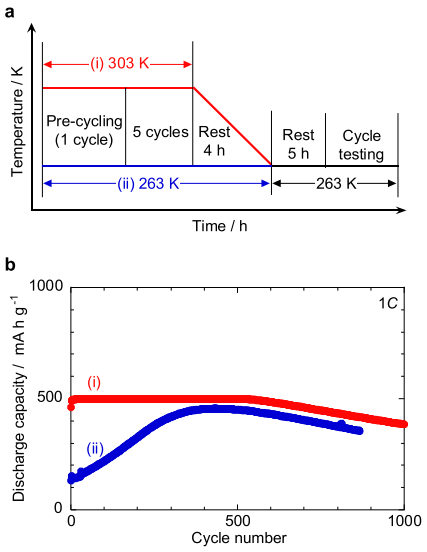

Figure 4. (a) Schematic process of the cycle life test at 263 K. The lithiation capacity was limited at 1000 and 500 mA h g^{-1} for five cycles after precycling and the cycle test, respectively. Precycling was performed at (i) 303 and (ii) 263 K. (b) Cycle life of the Si electrodes at 263 K in 1 M LiFSA/Py13-FSA with a lithiation capacity limit of 500 mA h g^{-1}.

Figure 5 provides the cycle life of a Si electrode at 263 K in ionic and organic liquid electrolytes with a charge capacity limitation of 500 mA h g^{-1}. In organic liquid electrolytes, an initial discharge capacity of 500 mA h g^{-1} was not obtained, which is an expected based on Figures 1b and 3 and Table 1. In contrast, the Si electrode maintained a reversible capacity of 500 mA h g^{-1} for over 150 and 500 cycles in 1 M LiFSA/EMI-FSA and 1 M LiFSA/Py13-FSA, respectively. We demonstrated that the cycle life of Si-based electrodes in FSA-based ionic liquid electrolytes was superior to that in conventional organic liquid electrolytes at room temperature.[17,20,21,50] In organic liquid electrolytes, a surface film with an inhomogeneous thickness forms on the electrode surface, and preferential Li^+ storage into Si occurs through thinner parts of the film. Inhomogeneous Li^+ storage prompts the local formation of a Li-rich Li−Si alloy phase, which causes local changes in the Si volume and electrode disintegration.[23] Conversely, in ionic liquid electrolytes, a surface film that includes LiF, which contributes to its mechanical and/or structural stability, forms by the rapid decomposition of the FSA anion;[61] thus, the surface film does not grow and remains uniform and thin at room temperature. The results indicate that homogeneous formation of a Li-poor Li−Si alloy phase occurs over the entire electrode, preventing the local accumulation of high strain.[23] Thus, severe Si electrode disintegration is suppressed. Additionally, the surface film formed in 1 M LiFSA/EMI-FSA should be thicker than that derived from the Py13-based electrolyte because EMI cation decomposition continually takes place in addition to FSA anion decomposition.[17,62,63] While we conducted the cycle test at the low temperature, surface film formation was performed at room temperature. Consequently, it was concluded that the cycle life at the low temperature was similar to that at room temperature and that the Si electrode exhibited a superior cycle life in 1 M LiFSA/Py13-FSA.

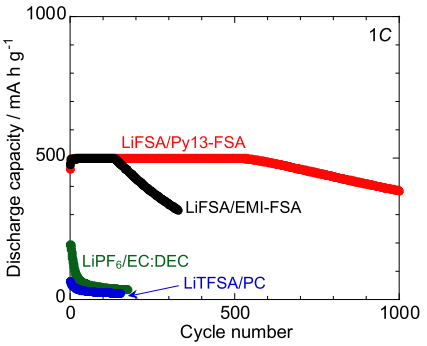

Figure 5. Cycle life of the Si electrodes at 263 K in various electrolytes with a charge capacity limitation of 500 mA h g^{-1}.

3.3. Impact of P-Doping into Si on Its Charge−Discharge Properties at Low Temperature.

We previously reported that the electrochemical performance of Si electrodes was improved by P-doping into Si.[19−21] The effect of P-doping on the performance improvement is explained as follows: (1) it suppresses the phase transition from Si into $Li_{15}Si_4$ due to shrinking the Si crystal lattice as a result of the replacement of some Si atoms with smaller P atoms; (2) it homogenizes the Li distribution because of faster Li diffusion within P-doped Si as a result of low electrical resistivity; and (3) it suppresses the Si volume expansion during its lithiation, which results from the above two effects.[19,21,23] We investigated the charge−discharge properties of a P-doped Si electrode at low temperatures. Figures S4 and S5 show changes in the reversible capacity of the 100 ppm P-doped Si electrode with decreasing temperature in various electrolytes and the corresponding charge−discharge curves, respectively. Compared to the Si electrode (Figure 1b), the capacity decay of the P-doped Si electrode with decreasing temperature was suppressed.

Figure 6 provides the cycle life of 100 ppm P-doped Si and Si electrodes at (a) 263 and (b) 303 K in 1 M LiFSA/Py13-FSA with a charge capacity limitation of 500 mA h g^{-1}. There was no significant difference between the charge−discharge

https://doi.org/10.1021/acsomega.2c00947
ACS Omega 2022, 7, 15846−15853

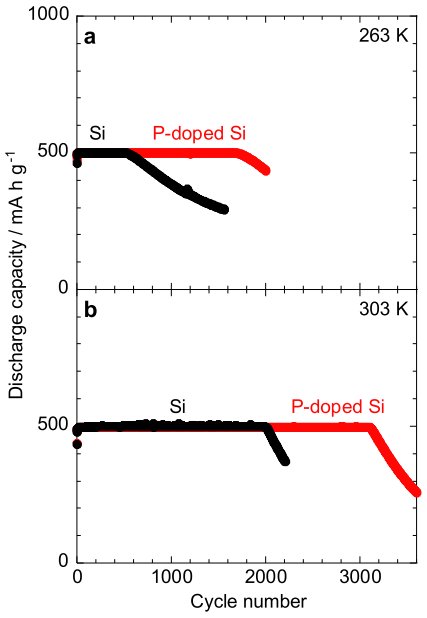

Figure 6. Cycle life of the 100 ppm P-doped Si and Si-only electrodes at (a) 263 and (b) 303 K in 1 M LiFSA/Py13-FSA with a charge capacity limitation of 500 mA h g^{-1}.

profiles of the electrodes at any temperature and cycle (Figure S6). The metallic luster of the counter electrode (Li metal) seemed to be slightly lost after the charge−discharge testing at 303 K, whereas white precipitates covered the electrode at 263 K. The appearance of the electrode after the testing differs depending on the temperature, but there is no difference at the same temperature (Figure S7); thus, the effect of the stripping and precipitation of the Li metal should be ignored. At 263 K, capacity fading of the Si- and P-doped Si electrodes occurred at approximately the 550th and 1710th cycles, respectively. Conversely, at 303 K, the Si- and P-doped Si electrodes exhibited capacity decay at approximately the 2000th and 3100th cycles, respectively. P-Doping into Si improved the cycle life of the electrode by approximately 3.1 times at low temperatures, whereas it was approximately 1.6 times at room temperature: the impact of P-doping into Si on the cycling performance improvement was more noticeable at low temperatures. Lithium diffusion changes within P-doped Si; thus it is considered that the shrinkage of the Si crystal lattice by P-doping contributes to the above improvement because the difference in temperature did not influence on the crystal lattice.

Figure 7 shows the cycle life of the 100 ppm P-doped Si electrode in various electrolytes at a lithiation capacity limitation of 500 mA h g^{-1}. In $LiPF_6$/EC+DEC, an initial discharge capacity of 500 mA h g^{-1} was obtained, whereas the Si electrode did not exhibit 500 mA h g^{-1} (Figure 5). In LiFSA/EMI-FSA, P-doping into Si improved the cycle life of the electrode by approximately 2.7 times, which is almost the same as the observed improvement in LiFSA/Py13-FSA. Hence, P-doping into Si enhanced the cycle life regardless of the electrolyte.

4. CONCLUSIONS

To use LIBs in various extreme environments, such as cold regions and outer space, we investigated the lithiation and delithiation properties of Si-based electrodes at low temperatures in ionic liquid electrolytes. The properties of the surface film on the electrodes and/or σ of the electrolytes determined the reversible capacity at low temperatures, and sufficient reversible capacity could not be obtained with a surface film formed at low temperatures. The electrodes exhibited superior cycle life in the ionic liquid electrolytes compared to conventional organic liquid electrolytes. The P-doped Si electrode had a cycle life at a low temperature (263 K) 3.1 times longer than that of the Si-only electrode, while it showed 1.6 times longer cycle life at room temperature (303 K). The effect of P-doping into Si on the cyclability improvement was more noticeable at low temperatures. Li diffusion changes within P-doped Si; thus, the shrinkage of the Si crystal lattice by P-doping may contribute to the above improvement because the difference in temperature did not influence the crystal lattice. Additionally, P-doping into Si enhanced the cycle life irrespective of the electrolyte. The obtained findings are essential for the practical application of LIBs using ionic liquid electrolytes.

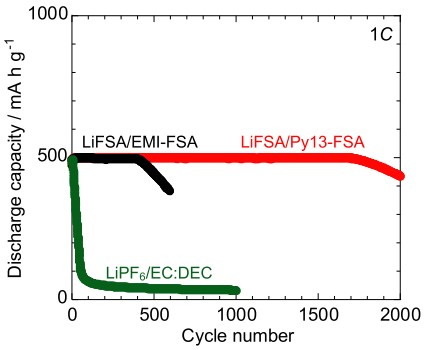

Figure 7. Cycle life of the 100 ppm P-doped Si electrodes at 263 K in various electrolytes with a charge capacity limitation of 500 mA h g^{-1}.

■ ASSOCIATED CONTENT

Supporting Information

The Supporting Information is available free of charge at https://pubs.acs.org/doi/10.1021/acsomega.2c00947.

Chemical structures, charge−discharge curves, temperature dependence of the discharge capacity, dQ/dV plots, and photographs of the counter electrodes (PDF)

■ AUTHOR INFORMATION

Corresponding Author

Hiroki Sakaguchi − *Department of Chemistry and Biotechnology, Graduate School of Engineering, Tottori University, Tottori 680-8552, Japan; Center for Research on Green Sustainable Chemistry, Tottori University, Tottori 680-8552, Japan;* orcid.org/0000-0002-4125-7182; Email: sakaguch@tottori-u.ac.jp

Authors

Yasuhiro Domi − *Department of Chemistry and Biotechnology, Graduate School of Engineering, Tottori University, Tottori 680-8552, Japan; Center for Research on Green Sustainable Chemistry, Tottori University, Tottori 680-8552, Japan;* orcid.org/0000-0003-3983-2202

Hiroyuki Usui − *Department of Chemistry and Biotechnology, Graduate School of Engineering, Tottori University, Tottori 680-8552, Japan; Center for Research on Green Sustainable*

https://doi.org/10.1021/acsomega.2c00947
ACS Omega 2022, 7, 15846−15853

Chemistry, Tottori University, Tottori 680-8552, Japan; orcid.org/0000-0002-1156-0340

Tasuku Hirosawa − *Center for Research on Green Sustainable Chemistry and Department of Engineering, Graduate School of Sustainability Science, Tottori University, Tottori 680-8552, Japan*

Kai Sugimoto − *Center for Research on Green Sustainable Chemistry and Department of Engineering, Graduate School of Sustainability Science, Tottori University, Tottori 680-8552, Japan*

Takuma Nakano − *Center for Research on Green Sustainable Chemistry and Department of Engineering, Graduate School of Sustainability Science, Tottori University, Tottori 680-8552, Japan*

Akihiro Ando − *Center for Research on Green Sustainable Chemistry and Department of Engineering, Graduate School of Sustainability Science, Tottori University, Tottori 680-8552, Japan*

Complete contact information is available at: https://pubs.acs.org/10.1021/acsomega.2c00947

Author Contributions

The manuscript was written with contributions from all authors.

Funding

This work was partially supported by the Japan Society for the Promotion of Science (JSPS) KAKENHI (Grant Nos. JP19K05649, JP19H02817, and JP20H00399).

Notes

The authors declare no competing financial interest.

■ ACKNOWLEDGMENTS

The authors thank Ms. R. Bamba for her kind assistance and ACS authoring services (https://authoringservices.acs.org/en/) for the English language review.

■ REFERENCES

(1) Yamagata, M.; Tanaka, K.; Tsuruda, Y.; Sone, Y.; Fukuda, S.; Nakasuka, S.; Kono, M.; Ishikawa, M. The First Lithium-ion Battery with Ionic Liquid Electrolyte Demonstrated in Extreme Environment of Space. *Electrochemistry* **2015**, *83*, 918−924.

(2) Yetik, O.; Karakoc, T. H. A Numerical Study on the Thermal Performance of Prismatic Li-ion Batteries for Hibrid Electric Aircraft. *Energy* **2020**, *195*, 117009.

(3) Lai, S. C. Solid Lithium-Silicon Electrode. *J. Electrochem. Soc.* **1976**, *123*, 1196−1197.

(4) Obrovac, M. N.; Christensen, L. Structural Changes in Silicon Anodes during Lithium Insertion/Extraction. *Electrochem. Solid-State Lett.* **2004**, *7*, A93−A96.

(5) Key, B.; Morcrette, M.; Tarascon, J.-M.; Grey, C. P. Pair Distribution Function Analysis and Solid State NMR Studies of Silicon Electrodes for Lithium Ion Batteries: Understanding the (De)lithiation Mechanisms. *J. Am. Chem. Soc.* **2011**, *133*, 503−512.

(6) Obrovac, M. N.; Krause, L. J. Reversible Cycling of Crystalline Silicon Powder. *J. Electrochem. Soc.* **2007**, *154*, A103−A108.

(7) Liu, X. H.; Zhong, L.; Huang, S.; Mao, S. X.; Zhu, T.; Huang, J. Y. Size-Dependent Fracture of Silicon Nanoparticles During Lithiation. *ACS Nano* **2012**, *6*, 1522−1531.

(8) Ding, N.; Xu, J.; Yao, Y. X.; Wegner, G.; Fang, X.; Chen, C. H.; Lieberwirth, I. Determination of the Diffusion Coefficient of Lithium Ions in Nano-Si. *Solid State Ionics* **2009**, *180*, 222−225.

(9) Xie, J.; Imanishi, N.; Zhang, T.; Hirano, A.; Takeda, Y.; Yamamoto, O. Li-Ion Diffusion in Amorphous Si Films Prepared by RF Magnetron Sputtering: A Comparison of Using Liquid and Polymer Electrolytes. *Mater. Chem. Phys.* **2010**, *120*, 421−425.

(10) McDowell, M. T.; Ryu, I.; Lee, S. W.; Wang, C.; Nix, W. D.; Cui, Y. Studying the Kinetics of Crystalline Silicon Nanoparticle Lithiation with In Situ Transmission Electron Microscopy. *Adv. Mater.* **2012**, *24*, 6034−6041.

(11) Liu, B.; Wang, X.; Chen, H.; Wang, Z.; Chen, D.; Cheng, Y.-B.; Zhou, C.; Shen, G. Hierarchical Silicon Nanowires-Carbon Textiles Matrix as a Binder-free Anode for High-performance Advanced Lithium-ion Batteries. *Sci. Rep.* **2013**, *3*, 1622.

(12) Yoon, T.; Bok, T.; Kim, C.; Na, Y.; Park, S.; Kim, K. S. mesoporous Silicon Hollow Nanocubes Derived from Metal-Organic Framework Template for Advanced Lithium-ion battery Anode. *ACS Nano* **2017**, *11*, 4808−4815.

(13) Hu, G.; Yu, R.; Liu, Z.; Yu, Q.; Zhang, Y.; Chen, Q.; Wu, J.; Zhou, L.; Mai, L. Surface Oxidation Layer-Mediated Conformal Carbon Coating on Si Nanoparticles for Enhanced Lithium Storage. *ACS Appl. Mater. Interfaces* **2021**, *13*, 3991−3998.

(14) Zhang, P.; Huang, L.; Li, Y.; Ren, X.; Deng, L.; Yuan, Q. Si/Ni_3Si-Encapulated Carbon Nanofiber Composites as Three-Dimensional Network Structured Anodes for Lithium-ion Batteries. *Electrochim. Acta* **2016**, *192*, 385−391.

(15) Domi, Y.; Usui, H.; Ueno, A.; Shindo, Y.; Mizuguchi, H.; Komura, T.; Nokami, T.; Itoh, T.; Sakaguchi, H. Effect of Annealing Temperature of Ni-P/Si on its Lithiation and Delithiation Properties. *J. Electrochem. Soc.* **2020**, *167*, 040512.

(16) Domi, Y.; Usui, H.; Nakabayashi, E.; Kimura, Y.; Sakaguchi, H. Effect of Element Substitution on Electrochemical Performance of Silicide/Si Composite Electrodes for Lithium-ion Batteries. *ACS Appl. Energy Mater.* **2020**, *3*, 7438−7444.

(17) Domi, Y.; Usui, H.; Shindo, Y.; Yodoya, S.; Sato, H.; Nishikawa, K.; Sakaguchi, H. Electrochemical Lithiation and Delithiation Properties of $FeSi_2$/Si Composite Electrode in Ionic-liquid Electrolytes. *Electrochemistry* **2020**, *88*, 548−554.

(18) Long, B. R.; Chan, M. K. Y.; Greeley, J. P.; Gewirth, A. A. Dopant Modulated Li Insertion in Si for Battery Anodes: Theory and Experiment. *J. Phys. Chem. C* **2011**, *115*, 18916−18921.

(19) Domi, Y.; Usui, H.; Shimizu, M.; Kakimoto, Y.; Sakaguchi, H. Effect of Phosphorus-doping on Electrochemical Performance of Silicon Negative Electrodes in Lithium-ion Batteries. *ACS Appl. Mater. Interfaces* **2016**, *8*, 7125−7132.

(20) Yodoya, S.; Domi, Y.; Usui, H.; Sakaguchi, H. Applicability of an Ionic Liquid Electrolyte to a Phosphorus-Doped Silicon Negative Electrode for Lithium-Ion Batteries. *ChemistrySelect* **2019**, *4*, 1375−1378.

(21) Domi, Y.; Usui, H.; Yamaguchi, K.; Yodoya, S.; Sakaguchi, H. Silicon-Based Anodes with Long Cycle Life for Lithium-Ion Batteries Achieved by Significant Suppression of Their Volume Expansion in Ionic-Liquid Electrolyte. *ACS Appl. Mater. Interfaces* **2019**, *11*, 2950−2960.

(22) Lau, D.; Hall, C. A.; Lim, S.; Yuwono, J. A.; Burr, P. A.; Song, N.; Lennon, A. Reduced Silicon Fragmentation in Lithium Ion Battery Anodes Using Electronic Doping Strategies. *ACS Appl. Energy Mater.* **2020**, *3*, 1730−1741.

(23) Domi, Y.; Usui, H.; Ando, A.; Nishikawa, K.; Sakaguchi, H. Analysis of the Li Distribution in Si-Based Negative Electrodes for Lithium-Ion Batteries by Soft X-ray Emission Spectroscopy. *ACS Appl. Energy Mater.* **2020**, *3*, 8619−8626.

(24) Shimizu, M.; Kimoto, K.; Kawai, T.; Taishi, T.; Arai, S. Dopant Effect on Lithiation/Delithiation of Highly Crystalline Silicon Synthesized Using the Czochralski Process. *ACS Appl. Energy Mater.* **2021**, *4*, 7922−7929.

(25) Domi, Y.; Usui, H.; Takaishi, R.; Sakaguchi, H. Lithiation and Delithiation Reactions of Binary Silicide Electrodes in an Ionic Liquid Electrolyte as Novel Anodes for Lithium-Ion Batteries. *ChemElectroChem.* **2019**, *6*, 581−589.

(26) Domi, Y.; Usui, H.; Sugimoto, K.; Gotoh, K.; Nishikawa, K.; Sakaguchi, H. Reaction Behavior of a Slicide Electrode with Lithium in an Ionic-liquid Electrolyte. *ACS Omega* **2020**, *5*, 22631−22636.

(27) Domi, Y.; Usui, H.; Nishikawa, K.; Sakaguchi, H. Metallographic Structure Changes in Lanthanum Slicide/Silicon Nanocomposite Electrodes during Lithiation and Delithiation: Implications for Battery Applications. *ACS Appl. Nano Mater.* **2021**, *4*, 8473−8481.
(28) Okubo, T.; Saito, M.; Yodoya, C.; Kamei, A.; Hirota, M.; Takenaka, T.; Okumura, T.; Tasaka, A.; Inaba, M. Effects of Li Pre-Doping on Charge/Discharge Properties of Si Thin Flakes as a Negative Electrode for Li-Ion Batteries. *Solid State Ionics* **2014**, *262*, 39−42.
(29) Domi, Y.; Usui, H.; Iwanari, D.; Sakaguchi, H. Effect of Mechanical Pre-Lithiation on Electrochemical Performance of Silicon Negative Electrode for Lithium-Ion Batteries. *J. Electrochem. Soc.* **2017**, *164*, A1651−A1654.
(30) Saito, M.; Kato, K.; Ishii, S.; Yoshii, K.; Shikano, M.; Sakaebe, H.; Kiuchi, H.; Fukunaga, T.; Matsubara, E. Effective Bulk Activation and Interphase Stabilization of Silicon Negative Electrode by Lithium Pre-Doping for Next-Generation Batteries. *J. Electrochem. Soc.* **2019**, *166*, A5174−A5183.
(31) Domi, Y.; Usui, H.; Ieuji, N.; Nishikawa, K.; Sakaguchi, H. Lithiation/Delithiation Properties of Lithium Silicide Electrodes in Ionic-liquid Electrolytes. *ACS Appl. Mater. Interfaces* **2021**, *13*, 3816−3824.
(32) Wang, J.; Yamada, Y.; Sodeyama, K.; Chiang, C. H.; Tateyama, Y.; Yamada, A. Superconcentrated Electrolytes for a High-Voltage Lithium-Ion Battery. *Nat. Commun.* **2016**, *7*, 12032.
(33) Yamaguchi, K.; Domi, Y.; Usui, H.; Shimizu, M.; Morishita, S.; Yodoya, S.; Sakata, T.; Sakaguchi, H. Effect of Film-Forming Additive in Ionic Liquid Electrolyte on Electrochemical Performance of Si Negative-Electrode for LIBs. *J. Electrochem. Soc.* **2019**, *166*, A268−A276.
(34) Matsumoto, K.; Hwang, J.; Kaushik, S.; Chen, C. Y.; Hagiwara, R. Advances in Sodium Secondary Batteries Utilizing Ionic Liquid Electrolytes. *Energy Environ. Sci.* **2019**, *12*, 3247−3287.
(35) Yamamoto, T.; Nohira, T. Tin Negative Electrodes Using an FSA-Based Ionic Liquid Electrolyte: Improved Performance of Potassium Secondary Batteries. *Chem. Commun.* **2020**, *56*, 2538−2541.
(36) Qi, H.; Ren, Y.; Guo, S.; Wang, Y.; Li, S.; Hu, Y.; Yan, F. High-Voltage Resistant Ionic Liquids for Lithium-Ion Batteries. *ACS Appl. Mater. Interfaces* **2020**, *12*, 591−600.
(37) Danzer, M. A.; Petzl, M. Nondestructive Detection, Characteriation and Quantification of Lithium Plating in Commercial Lithium-ion Batteries. *J. Power Sources* **2014**, *254*, 80−87.
(38) Jones, J.-P.; Smart, M. C.; Krause, F. C.; Bugga, R. V. The Effect of Electrolyte Additives upon Lithium Plating during Low Temperature Charging of Graphite-LiNiCoAlO$_2$ Lithium-ion Three Electrode Cells. *J. Electrochem. Soc.* **2020**, *167*, 020536.
(39) Nakagawa, H.; Shibata, Y.; Fujino, Y.; Tabuchi, T.; Inamasu, T.; Murata, T. Application of Nonflammable Electrolytes to High Performance Lithium-ion Cells. *Electrochemistry* **2010**, *78*, 406−408.
(40) Nakagawa, H.; Domi, Y.; Doi, T.; Ochida, M.; Tsubouchi, S.; Yamanaka, T.; Abe, T.; Ogumi, Z. In Situ Raman Study of Graphite Negative-Electrodes in Electrolyte Solution Containing Fluorinated Phosphoric Esters. *J. Electrochem. Soc.* **2014**, *161*, A480−A485.
(41) Earle, M. J.; Esperança, J. M. S. S.; Gilea, M. A.; Canongia Lopes, J. N.; Rebelo, L. P. N.; Magee, J. W.; Seddon, K. R.; Widegren, J. A. The Distillation and Volatility of Ionic Liquids. *Nature* **2006**, *439*, 831−834.
(42) Hapiot, P.; Lagrost, C. Electrochemical Reactivity in Room-Temperature Ionic Liquids. *Chem. Rev.* **2008**, *108*, 2238−2264.
(43) Sippel, P.; Lunkenheimer, P.; Krohns, S.; Thoms, E.; Loidl, A. Importance of Liquid Fragility for Energy Applications of Ionic Liquids. *Sci. Rep.* **2015**, *5*, 13922.
(44) Ghoufi, A.; Szymczyk, A.; Malfreyt, P. Ultrafast diffusion of Ionic Liquids Confined in Carbon Nanotubes. *Sci. Rep.* **2016**, *6*, 28518.
(45) Men, F.; Yang, Y.; Shang, Y.; Zhang, H.; Song, Z.; Zhou, Y.; Zhou, X.; Zhan, H. Fluorine-Substituted Ionic Liquid for Si Anode in Li-Ion Battery. *J. Power Sources* **2018**, *401*, 354−361.
(46) Arano, K.; Mazouzi, D.; Kerr, R.; Lestriez, B.; Le Bideau, J.; Howlett, P. C.; Dupre, N.; Forsyth, M.; Guyomard, D. Understanding the Superior Cycling Performance of Si Anode in Highly Concentrated Phosphonium-based Ionic Liquid Electrolyte. *J. Electrochem. Soc.* **2020**, *167*, 120520.
(47) Wang, H.; Tao, T.; Xu, J.; Mei, X.; Liu, X.; Gou, P. Cooling Capacity of a Novel Modular Liquid-cooled Battery Thermal Management System for Cylindrical Lithium Ion Batteries. *Appl. Therm. Eng.* **2020**, *178*, 115591.
(48) Subburaj, T.; Brevet, W.; Farmakis, F.; Tsiplakides, D.; Balomenou, S.; Strataki, N.; Elmasides, C.; Samaniego, B.; Nestoridi, M. Silicon/LiNi$_{0.8}$Co$_{0.15}$Al$_{0.05}$O$_2$ Lithium-ion Pouch Cells Charging and Discharging at −40°C Temperature. *Electrochim. Acta* **2020**, *354*, 136652.
(49) Richter, K.; Waldmann, T.; Paul, N.; Jobst, N.; Scurtu, R.-G.; Hofmann, M.; Gilles, R.; Wohlfahrt-Mehrens, M. Low-temperature Charging and Aging Mechanisms of Si/C Composite Anodes in Li-ion Batteries: an Operando Neutron Scattering Study. *ChemSusChem* **2020**, *13*, 529−538.
(50) Domi, Y.; Usui, H.; Shindo, Y.; Ando, A.; Sakaguchi, H. Lithiation and Delithiation Properties of Si-based Electrodes Pre-coated with a Surface Film Derived from an Ionic-liquid Electrolyte. *Chem. Lett.* **2021**, *50*, 1041−1044.
(51) Domi, Y.; Usui, H.; Sugimoto, K.; Sakaguchi, H. Effect of Silicon Crystallite Size on Its Electrochemical Performance for Lithium-ion Batteries. *Energy Technology* **2019**, *7*, 1800946.
(52) Nakamura, H.; Komatsu, H.; Yoshio, M. Suppression of Electrochemical Decomposition of Propylene Carbonate at a Graphite Anode in Lithium-ion Cells. *J. Power Sources* **1996**, *62*, 219−222.
(53) Wrodnigg, G.; Besenhard, J. O.; Winter, M. Ethylene Sulfite as Electrolyte Additive for Lithium-ion Cells with Graphitic Anodes. *J. Electrochem. Soc.* **1999**, *146*, 470−472.
(54) Jones, J.; Anouti, M.; Caillon-Caravanier, M.; Willmann, P.; Sizaret, P.-Y.; Lemordant, D. Solubilization of SEI Lithium Salts in Alkylcarbonate Solvents. *Fluid Phase Equilib.* **2011**, *305*, 121−126.
(55) Atik, J.; Röser, S.; Wagner, R.; Berghus, D.; Winter, M.; Cekic-Laskovic, I. Acyclic Acetals in Propylene Carbonate-based Electrolytes for Advanced and Safer Graphite-based Lithium Ion Batteries. *J. Electrochem. Soc.* **2020**, *167*, 040509.
(56) Uchida, S.; Katada, T.; Ishikawa, M. Impact of Lithium-ion Coordination in Carbonate-based Electrolyte on Lithium-ion Intercalation Kinetics into Graphite Electrode. *Electrochem. Commun.* **2020**, *114*, 106705.
(57) Evans, T.; Olson, J.; Bhat, V.; Lee, S.-H. Effect of Organic Solvent Addition to PYR$_{13}$FSI + LiFSI Electrolytes on Aluminum Oxidation and Rate Performance of Li(Ni$_{1/3}$Mn$_{1/3}$Co$_{1/3}$)O$_2$ Cathodes. *J. Power Sources* **2014**, *265*, 132−139.
(58) Hirota, N.; Okuno, K.; Majima, M.; Hosoe, A.; Uchida, S.; Ishikawa, M. High-performance Lithium-ion Capacitor Composed of Electrodes with Porous Three-dimensional Current Collector and Bis(fluorosulfonyl)imide-based Ionic Liquid Electrolyte. *Electrochim. Acta* **2018**, *276*, 125−133.
(59) Matsumoto, K.; Nishiwaki, E.; Hosokawa, T.; Tawa, S.; Nohira, T.; Hagiwara, R. Thermal, Physical, and Electrochemical Properties of Li[N(SO$_2$F)$_2$]-[1-Ethyl-3-methylimidazolium][(SO$_2$F)$_2$] Ionic Liquid Electrolytes for Li Secondary Batteries Operated at Room and Intermediate Temperatures. *J. Phys. Chem. C* **2017**, *121*, 9209−9219.
(60) Chung, G. J.; Han, J.; Song, S.-W. Fire-preventing LiPF$_6$ and Ethylene Carbonate-based Organic Liquid Electrolyte System for Safer and Outperforming Lithium-ion Batteries. *ACS Appl. Mater. Interfaces* **2020**, *12*, 42868−42879.
(61) Piper, D. M.; Evans, T.; Leung, K.; Watkins, T.; Olson, J.; Kim, S. C.; Han, S. S.; Bhat, V.; Oh, K. H.; Buttry, D. A.; Lee, S. H. Stable Silicon-Ionic Liquid Interface for Next-Generation Lithium-Ion Batteries. *Nat. Commun.* **2015**, *6*, 6230.
(62) Sugimoto, T.; Kikuta, M.; Ishiko, E.; Kono, M.; Ishikawa, M. Ionic Liquid Electrolytes Compatible with Graphitized Carbon

https://doi.org/10.1021/acsomega.2c00947
ACS Omega 2022, 7, 15846−15853

Negative without Additive and their effects on Interfacial Properties. *J. Power Sources* **2008**, *183*, 436−440.
(63) Sugimoto, T.; Atsumi, Y.; Kono, M.; Kikuta, M.; Ishiko, E.; Yamagata, M.; Ishikawa, M. Application of bis(fluorosulfonyl)imide-based Ionic Liquid Electrolyte to Silicon-Nickel-Carbon Composite Anode for Lithium-ion Batteries. *J. Power Sources* **2010**, *195*, 6153−6156.

https://doi.org/10.1021/acsomega.2c00947
ACS Omega 2022, 7, 15846−15853